Is Assembly of the SNARE Complex Enough to Fuel Membrane Fusion?[s]

Katrin Wiederhold[1] and Dirk Fasshauer[2]

From the Research Group Structural Biochemistry, Department of Neurobiology, Max Planck Institute for Biophysical Chemistry, Am Fassberg 11, 37077 Göttingen, Germany

The three key players in the exocytotic release of neurotransmitters from synaptic vesicles are the SNARE (soluble *N*-ethylmaleimide-sensitive factor attachment protein receptor) proteins synaptobrevin 2, syntaxin 1a, and SNAP-25. Their assembly into a tight four-helix bundle complex is thought to pull the two membranes into close proximity. It is debated, however, whether the energy generated suffices for membrane fusion. Here, we have determined the thermodynamic properties of the individual SNARE assembly steps by isothermal titration calorimetry. We found extremely large favorable enthalpy changes counterbalanced by positive entropy changes, reflecting the major conformational changes upon assembly. To circumvent the fact that ternary complex formation is essentially irreversible, we used a stabilized syntaxin-SNAP-25 heterodimer to study synaptobrevin binding. This strategy revealed that the N-terminal synaptobrevin coil binds reversibly with nanomolar affinity. This suggests that individual, membrane-bridging SNARE complexes can provide much less pulling force than previously claimed.

The molecular machinery that drives the Ca^{2+}-dependent release of neurotransmitters from synaptic vesicles is studied intensively. Three key players in the underlying exocytotic fusion of the vesicle with the plasma membrane are the proteins synaptobrevin 2/VAMP2 (vesicle-associated membrane protein), syntaxin 1a, and SNAP-25[3] (for review, see Refs. 1–7). They belong to the so-called SNARE protein family, the members of which are involved in all vesicle fusion steps in the endocytic and secretory pathway. In general, SNARE proteins are relatively small, tail-anchored membrane proteins. Their key characteristic is the so-called SNARE motif, an extended stretch of heptad repeats that is usually connected to a single transmembrane domain by a short linker. Syntaxin and synaptobrevin each contain a single SNARE motif, whereas SNAP-25 contains two SNARE motifs connected by a palmitoylated linker region serving as a membrane anchor. The SNARE motifs of the three proteins assemble into a very tight four-helix bundle between opposing membranes; during this process the plasma membrane proteins syntaxin and SNAP-25 provide the binding site for the vesicular synaptobrevin. Formation of this complex is accompanied by extensive structural rearrangements (8–10). Based on these findings, it was put forward that the formation of the SNARE bundle provides the energy that drives membrane fusion. As the bundle is oriented in parallel, it is thought that formation of this complex starts from the membrane-proximal N termini and proceeds toward the C-terminal membrane anchors, effectively pulling the membranes together (the "zipper" model) (11). Although the zipper scenario is intuitive, it has been difficult to demonstrate directly.

A decade ago it was shown that the three neuronal SNARE proteins are sufficient to fuse artificial vesicles (12). However, this reductionist approach yields rather slow fusion rates (12–14). Over the years various different end products of SNARE catalysis (complete fusion, hemifusion, and only tethered membranes) have been reported (15–19). These unsatisfactory results have fueled the debate over whether the assembly process indeed provides enough impetus to fuse bilayers. Not surprisingly, an alternative scenario has been put forward in which repulsive forces between membranes bring the SNARE assembly to a grinding halt. According to this idea, other factors like the Ca^{2+} sensor synaptotagmin or the small soluble protein complexin are needed to induce membrane merging (20–22).

In simple terms, to find out whether the SNARE complex assembly is enough for membrane fusion, only the amount of energy released during complex formation and the amount of energy needed for membrane fusion need to be compared. However, the physics of membrane fusion are very complicated, and it is even more challenging to understand how proteins modulate the process. The free energy for bilayer fusion in an aqueous environment is not very high, but fusion is thought to require a large activation energy of about 40 k_BT, as two charged membranes have to be brought into close apposition. According to a theoretical model, the apposing membranes then need to be modified into a stalk-like configuration. Before fusion occurs, the process is thought to pass through a hemifusion intermediate in which only the outer monolayers are merged (for review, see Refs. 23 and 24). The role of fusion proteins is thought to lower the energy barrier for membrane fusion, but understanding how they modulate the lipid membrane and how their conformational changes are translated into a mechanical force is still in its infancy. It is not clear, for instance, whether SNARE-catalyzed fusion indeed proceeds through a stalk-like structure or just locally alters the membranes, a mechanism that might need much less activation energy.

Energetics of SNARE Complex Formation

As the folding and unfolding transitions of the ternary SNARE complex exhibit a marked hysteresis (25), the question of how much energy is released during complex formation has been difficult to answer as well. To avoid the quasi-irreversibility of the process, the problem has been elegantly tackled by atomic force microscopy by two different research groups (26–28). In these experiments individual complexes affixed to solid supports were ruptured, yielding energy values of 43 and 33 $k_B T$. In another approach, which used a surface-force apparatus (SFA), a comparable energy of 35 $k_B T$ has recently been determined (29). Strikingly, these values appear to correspond closely with the activation energy needed to fuse two membranes, substantiating the view that SNAREs are nano-fusion machineries. However, one should be cautious about the conclusion that these sophisticated procedures in fact yield the genuine SNARE assembly energy. For example, with the SFA approach, the number of complexes had to be deduced rather indirectly to estimate the free energy. Moreover, these approaches offered only indirect information about the reaction pathway.

In this study we set out to determine the SNARE assembly energy more directly by using isothermal titration calorimetry (ITC) complemented by kinetic measurements. ITC is a powerful technique for studying the thermodynamics of macromolecular interactions by directly measuring the heat changes associated with complex formation, which at constant pressure is equal to the enthalpy change (ΔH). The titration approach also yields the stoichiometry (n), the entropy change (ΔS), and the association constant (K_A) of the reaction. We studied the consecutive reaction steps individually to gain deeper insights into the rugged energy landscape of complex formation. To study synaptobrevin binding in isolation, we used a stabilized syntaxin-SNAP-25 heterodimer, which has been shown to greatly accelerate liposome fusion rates (30). This strategy revealed that the N-terminal coil of synaptobrevin binds reversibly, making it feasible to access the free energy of SNARE assembly. Overall, our results suggest that individual SNARE complexes might provide much less pulling energy than previously claimed.

EXPERIMENTAL PROCEDURES

Protein Constructs—All recombinant proteins were derived from cDNAs from rat. The basic SNARE expression constructs cysteine-free SNAP-25A (residues 1–206), the syntaxin 1A SNARE motif (SyxH3, residues 180–262), the soluble domain of synaptobrevin 2 (Syb-(1–96)), and a few shortened synaptobrevin constructs have been described before; Syb-(49–96) and Syb-(49–96) contain a single cysteine residue at position 79 (Syb-(49–96)$^{Cys-79}$) for fluorescence labeling (25, 30, 31). Additional truncated versions of synaptobrevin were cloned into the pET28a vector: Syb-(1–87), Syb-(1–70), Syb-(1–65), Syb-(1–52). Note that the constructs Syb-(1–87) and Syb-(1–52) each contain an additional C-terminal Cys residue, residues 88 and 53, respectively, for fluorescence labeling.

Protein Purification—All proteins were expressed in *Escherichia coli* strain BL21 (DE3) and purified by Ni^{2+}-nitrilotriacetic acid chromatography followed by ion exchange chromatography on an Äkta system (GE Healthcare) essentially as

described (57). His$_6$ tags were generally removed using thrombin. All SNARE complexes were purified using a Mono Q column (GE Healthcare) after overnight assembly of the purified monomers. The following ternary complexes were employed: Syb-(49–96)·SyxH3·SNAP-25 (ΔN complex), Syb-(49–96)$^{Cys-79}$· SyxH3·SNAP-25, Syb-(1–52)·SyxH3·SNAP-25 (Syb-(1–52) complex), and Syb-(1–70)·SyxH3·SNAP-25 (Syb-(1–70) complex). The peptide comprising the C-terminal region of synaptobrevin (Syb-(71–96)) and a similar peptide containing an additional C-terminal Cys residue (Syb-(71–96)$^{Cys-79}$) were synthesized. Protein concentrations were determined by absorption at 280 nm in 6 M guanidine hydrochloride and/or using the Bradford assay.

ITC—ITC was performed on a VP-ITC instrument (Microcal) at 25 °C essentially as described (51). Samples were dialyzed twice against a degassed phosphate buffer (20 mM sodium phosphate, pH 7.4, 150 mM NaCl, 1 mM dithiothreitol). Typically, an initial 5-μl injection was followed by several 15-μl injections. The heat change per injection was integrated to yield the molar enthalpy for each injection. Blank titrations, which were carried out by injection of the ligand into a buffer, were subtracted from each data set. Note that we had to use relatively long equilibration times (300–1500 s) to record the slow binding reaction between SNARE proteins. In addition, we noticed that with further injections, the time required for the ΔT signal to return to the base line after an injection peak deflection was getting longer, rendering it necessary to extend the spacing between injections. All ITC experiments were carried out at least twice. The resulting binding isotherms were analyzed using the Microcal Origin ITC software package to obtain the binding enthalpy (ΔH), the stoichiometry (n), and the association constant (K_A). Depending on the reaction investigated, we used either a "one-set-of-sites" binding model that assumes that one or more ligands bind with similar affinities or a "two-sets-of-sites" binding model that assumes two sites with different values of K_A and ΔH. The dissociation constant (K_D) and the binding free energy (ΔG) were calculated using the basic thermodynamic relationships $K_D = K_A^{-1}$, $\Delta G = -RT \ln K_A$, and $\Delta G = \Delta H - T\Delta S$. Note that because of the limitations of the standard ITC analysis method, the contributions of sequential reaction steps cannot be resolved completely. ΔH *versus* T plots were fitted to the equation $\Delta H = \Delta Cp\ (T - T_{\Delta H = 0})$, where ΔCp is the heat capacity change of binding, and $T_{\Delta H = 0}$ is a reference temperature at which $\Delta H = 0$.

Fluorescence Spectroscopy—All measurements were carried out in a Fluorolog 3 spectrometer in T-configuration equipped for polarization (Model FL322, Horiba Jobin Yvon). Single cysteine variants were labeled with Texas Red C5 bromoacetamide or Alexa-488 C5 maleimide according to the manufacturer's instructions (Invitrogen). All experiments were performed at 25 °C in 1-cm quartz cuvettes (Hellma) in a phosphate buffer. Measurements of the fluorescence anisotropy, which reports the local flexibility of the labeled residue and which increases upon complex formation and decreases upon dissociation, were carried essentially as described (30, 31). The G factor was calculated according to $G = I_{HV}/I_{HH}$, where I is the fluorescence intensity, the first subscript letter indicates the direction of the exciting light, and the second subscript indicates the let-

ter the direction of emitted light. The intensities of the vertically (V) and horizontally (H) polarized emission light after excitation by vertically polarized light were measured. The anisotropy (r) was determined according to $r = (I_{VV} - GI_{VH})/(I_{VV} + 2 GI_{VH})$.

Circular Dichroism (CD) Spectroscopy—Measurements were performed essentially as described (25, 30, 31) using a Chirascan instrument (Applied Photophysics). Hellma quartz cuvettes with a path length of 0.1 cm were used. The far-UV spectra were obtained using steps of 1 nm with a scan rate of 60 nm/min and an averaging time of 0.5–2 s. For spectral measurements, different protein combinations at a concentration of about 5–10 μM in phosphate buffer were incubated overnight. The measurements were carried out at 25 °C. For thermal denaturation experiments, the purified complexes were dialyzed against phosphate buffer. The ellipticity at 222 nm was recorded between 25 and 95 °C at temperature increments of 30 °C/h.

RESULTS

In ITC experiments, two macromolecules, one in a thermally insulated cell and the other in a syringe, are sequentially mixed at a constant temperature. ITC is, therefore, well suited to monitor reversible bimolecular reactions. Because neuronal SNARE complex formation occurs by interaction of the three molecules, it was necessary to investigate each individual binary binding step first. The assembly pathway of the ternary SNARE complex is illustrated in Fig. 1a. This information then served as a basis to dissect the ternary SNARE complex reaction further by using a stabilized syntaxin-SNAP-25 heterodimer as a binding site for synaptobrevin (30). Eventually, this stabilized acceptor complex allowed the quasi-irreversibility (25) of the whole reaction to be avoided.

Large Enthalpic Change Observed within Assembly of the SNARE Complex—At first we investigated all possible binary combinations of the three neuronal SNARE proteins. For the experiments, we used full-length SNAP-25A and the entire cytosolic portion of synaptobrevin, Syb-(1–96). As the N-terminal autonomously folded region of syntaxin 1a is not part of the core SNARE complex, we employed a construct bearing only the SNARE motif (also referred to as the H3-domain) of syntaxin (SyxH3) for our studies. Titrations of synaptobrevin into SyxH3 (step 1.1) or into SNAP-25 (step 1.3) produced only background heat of dilution, whereas large heat changes were detected upon titration of SNAP-25 and SyxH3 (step 1.2 and 2.1, Fig. 1b). This is consistent with earlier CD and fluorescence measurements that had shown that only syntaxin and SNAP-25 form a stable binary complex that exhibits a 2:1 stoichiometry (8, 31). The result of a typical ITC experiment, in which SNAP-25 was titrated into syntaxin, is shown in Fig. 1b. With progressive injections, the heat signal diminished, saturating at a molar ratio of ≈0.65, corroborating the formation of a complex with 2:1 stoichiometry. A striking feature of this interaction is the enormously favorable binding energy per mole of injected SNAP-25, suggesting that a large number of binding interactions are established. This enormous enthalpic change was counterbalanced by a large positive entropy change,

reflecting the disorder-to-order transition during complex formation.

As this approach did not clearly disclose two consecutive binding steps, we next swapped the contents of the cell and the syringe by injecting SyxH3 into SNAP-25. In this manner, a transient 1:1 heterodimer is more likely to be detected, as SyxH3 is first injected into a large excess of SNAP-25 that shifts the equilibrium toward the formation of the 1:1 heterodimer. Indeed, the resulting ITC profile of this titration exhibited two distinct binding steps (Fig. 1c). This binding equilibrium was approximately evaluated with the two-sets-of-sites model that assumes the two binding sites have different affinities and enthalpies. Binding of the first SyxH3 molecule to SNAP-25 occurred with high affinity ($K_D \approx 5$ nM, step 1.2), whereas the second SyxH3 associates at moderate affinity (K_D of ≈ 234 nM, step 2.1). This agrees well with our earlier kinetic investigations that had suggested that the first SyxH3 molecule binds with a K_D of ≈ 16 nM to SNAP-25 (Fig. 1a) (31).

In the next set of experiments we monitored the formation of the ternary SNARE complex by injecting SNAP-25 into a stoichiometrically mixed 1:1 solution of the non-interacting constituents syntaxin and synaptobrevin (step 1.2 and 2.2). Fig. 1d shows a typical ITC titration of SNAP-25 into a premix of SyxH3 and Syb-(1–96). These data reveal that upon ternary SNARE complex formation, even larger enthalpic changes occurred ($\Delta H° \approx 110$ kcal/mol SNAP-25) than were observed for the interaction of syntaxin and SNAP-25. This very probably reflects the even more pronounced structural changes coupled to assembly of the ternary SNARE complex as compared with the assembly of syntaxin and SNAP-25. As we observed in the formation of the syntaxin-SNAP-25 complex, the large enthalpic changes upon assembly of the ternary complex were balanced by large entropic changes. This is also reflected in the large negative heat capacity change of binding (ΔCp, supplemental Fig. 1). In agreement with the composition of the ternary SNARE complex, saturation of binding occurred at a molar ratio of ≈1, consistent with a 1:1:1 composition of the complex. We also found clear evidence for a two-step assembly process for the ternary interaction when we titrated a mix of SyxH3 and Syb-(1–96) into SNAP-25 (Fig. 1e), confirming that synaptobrevin binds to the preassembled 1:1 syntaxin-SNAP-25 heterodimer (30, 31).

Isolating the Synaptobrevin Binding Step—So far, our ITC measurements have revealed that SNARE complex formation is accompanied by major enthalpic changes but did not reveal the free energy of the process. In fact, as the assembly is quasi-irreversible (25), a conventional thermodynamic analysis of the ITC data is not possible. However, an estimate of the $K_D \approx 10$ nM was achieved by fitting the data provisionally to a one-site binding model. It should be kept in mind, however, that the actual affinity of the ternary SNARE complex might be higher. To overcome this problem, we set out to investigate the association of synaptobrevin (step 2.2) in more detail, as this step of the reaction cascade seems to establish the irreversibility of the assembly process. However, synaptobrevin binding is difficult to study individually because the complex of the two proteins syntaxin and SNAP-25, as shown in the previous section, resides in a dynamic equilibrium between a 1:1 and a 2:1 stoi-

Energetics of SNARE Complex Formation

chiometry, depending on the mixing ratio. As an alternative, the syntaxin-SNAP-25 heterodimer can be stabilized artificially by a short C-terminal fragment of synaptobrevin. This so-called "ΔN" complex can be purified. As we have demonstrated earlier, the ΔN complex offers an accessible binding site for synaptobrevin but does not allow for binding of a second syntaxin. In a second step, the C-terminal peptide is quickly displaced from the ΔN complex (30). The assembly pathway using the ΔN complex is illustrated in Fig. 2a.

For our ITC experiments, we purified a ΔN complex containing a fragment of synaptobrevin encompassing the residues 49–96 (Syb-(49–96)·SyxH3·SNAP-25 complex). When we titrated Syb-(1–96) into the ΔN complex, we detected favorable enthalpic changes of ≈30 kcal/mol (Fig. 2b). This enthalpic change was markedly reduced in comparison to the ITC titrations in which all three constituents were mixed (Fig. 1c). Because synaptobrevin in this setting probably binds to a prestructured binding site in the ΔN complex, the enthalpic changes might to a large degree reflect coupled folding and binding of the synaptobrevin coil. We fitted the data to a one-site binding model, yielding an apparent affinity of ≈2 nM. However, it should be pointed out again that this value might not correspond completely with the genuine affinity of the SNARE complex. The reason is that binding of synaptobrevin is followed by a second reaction by which the C-terminal fragment is displaced. Thus, at the end of this assembly pathway, the same quasi-irreversible product is formed (Fig. 2a). Moreover, it seemed possible the displacement of the fragment might render the assembly pathway via the ΔN complex energetically less efficient. On the other hand, greatly enhanced fusion rates are observed using the ΔN complex compared with the use of the preassembled binary syntaxin-SNAP-25 complex, dem-
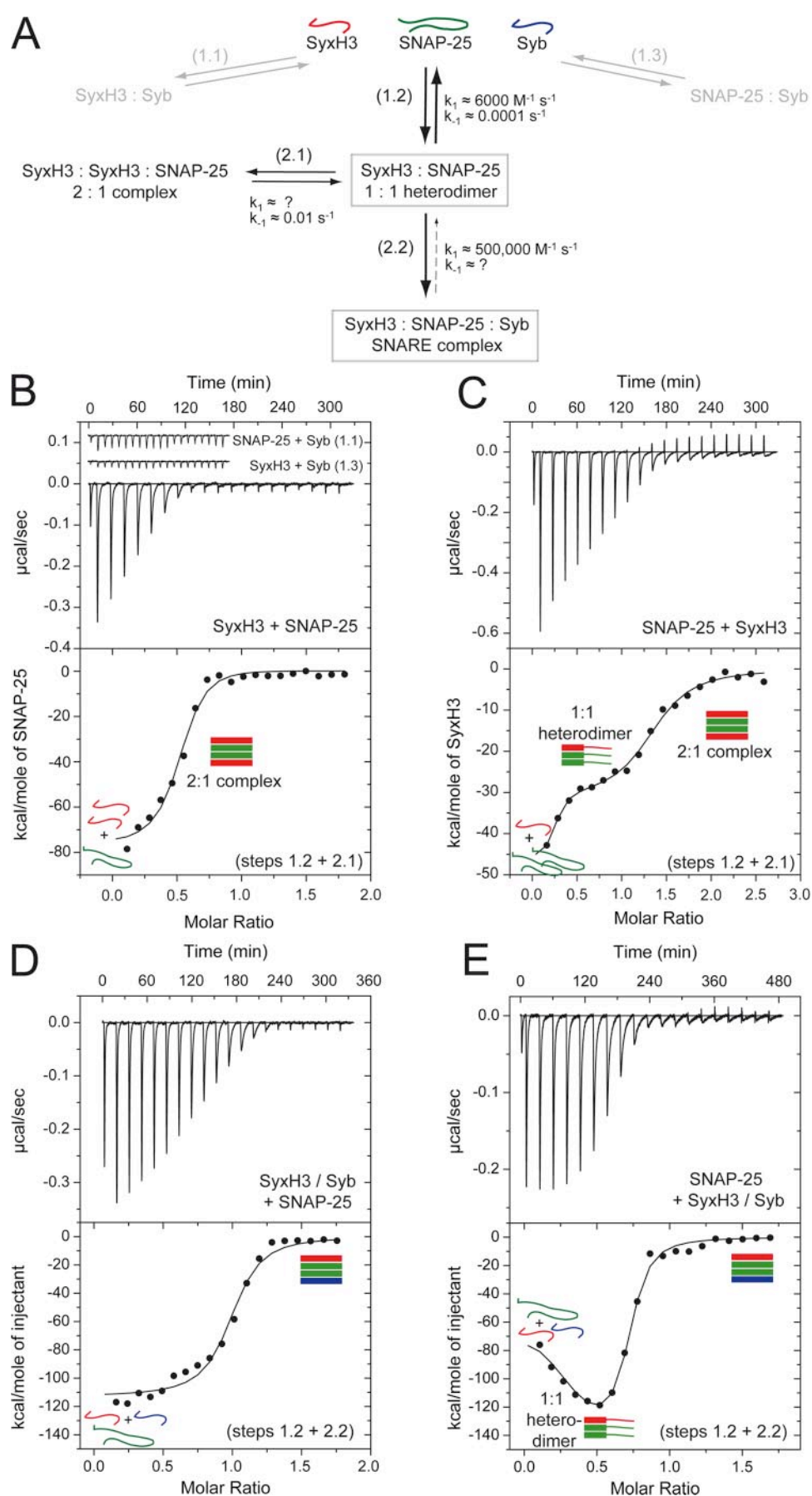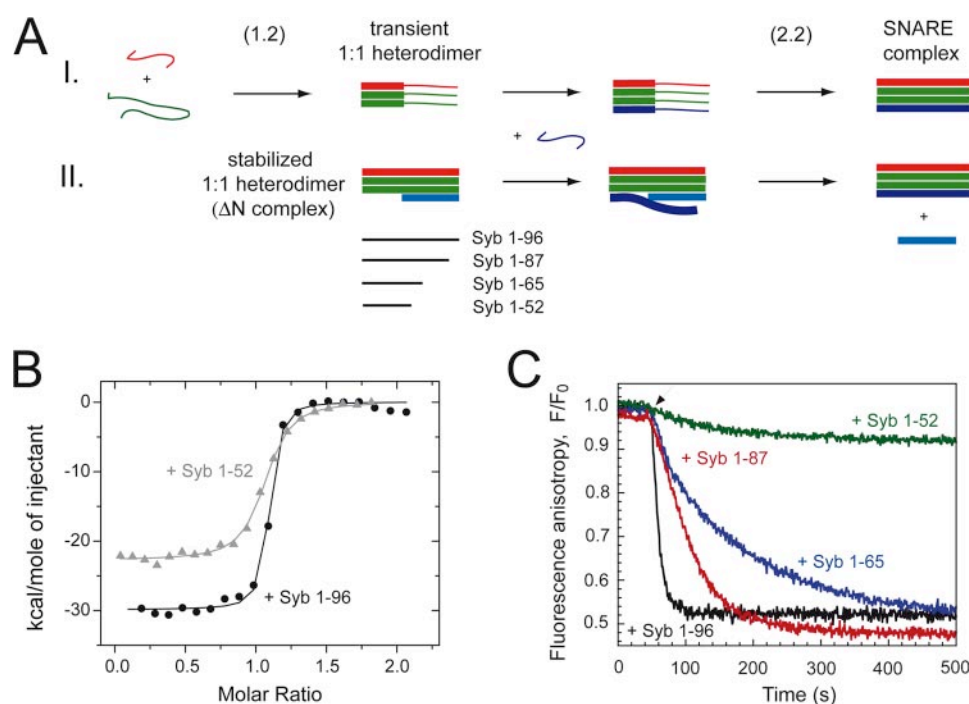
FIGURE 2. **Binding of the N-terminal coil of synaptobrevin to the ΔN complex is reversible.** *a*, comparative depiction of the SNARE assembly pathways using individual proteins (*I*) or the ΔN complex (*II*). *b*, titration of Syb-(1–96) (15 μM, *closed circles*) and of Syb-(1–52) (20 μM, *gray triangles*) into the purified ΔN complex (Syb-(49–96)·SyxH3·SNAP-25; 1.7 μM). This reaction only approximately corresponds to the interaction of synaptobrevin with the 1:1 heterodimer (step 2.2) because the C-terminal Syb-(49–96) fragment is displaced after N-terminal binding. Note that binding of synaptobrevin to the ΔN complex is relatively quick, making the reaction easier to follow by ITC as the stoichiometric mix of all three complex components. *c*, active displacement of Syb-(49–96) from the ΔN complex. To record displacement, we used a strategy employed earlier (30). Basically, we followed the dissociation of fluorescently labeled Syb-(49–96) fragment from the ΔN complex, which was visible by a decrease in fluorescence anisotropy. About 100 nM concentrations of a ternary complex containing Alexa-488-labeled Syb-(49–96) (Syb-(49–96)$^{Cys-79-Alexa-488}$·SyxH3·SNAP-25) was incubated with different Syb fragments (500 nM). The addition of Syb-(1–52) did not displace the fragment, whereas longer fragments dislodged the labeled fragment. In agreement with our previous findings (30), the labeled fragment was quickly displaced upon the addition of the entire cytoplasmic domain of synaptobrevin, Syb-(1–96). Displacement was already significantly slower when a synaptobrevin construct that lacked the eight C-terminal residues (Syb-(1–87)) was used, probably demonstrating that the synaptobrevin membrane-adjacent region contributes to binding strength. We still observed displacement, albeit much less efficiently, when 31 C-terminal residues were truncated. Thus, the longer the overlapping region, the more efficiently displacement occurs. This suggests that displacement is an active process in which the C-terminal, overlapping region dislodges the Syb-(49–96) fragment from the ΔN complex.

onstrating that this reaction pathway provides enough impetus to fuse artificial membranes (30).

The question arose as to how much of the observed enthalpy change upon binding of Syb-(1–96) to the ΔN complex reflects only the association of the N-terminal coil of synaptobrevin with the open N-terminal site and how much heat is released during the subsequential displacement step.

It seemed possible that this step does not significantly contribute to the thermal profile of the reaction, as the C-terminal portion of the displacing Syb-(1–96) is virtually identical to the displaced fragment (Syb-(49–96)). We, thus, sought an experimental strategy to isolate the thermodynamic parameters of the binding event. When we examined several C-terminally truncated synaptobrevin constructs, we found that a fragment comprising only the amino acids 1–52 (Syb-(1–52)) was incapable of displacing the Syb-(49–96) fragment (Fig. 2*c*). This observation suggests that both N- and C-terminal fragments of synaptobrevin can bind simultaneously, forming a Syb-(1–52)-Syb-(49–96) complex, although few amino acids overlap in this assembly. To rule out the possibility that the labeled Syb-(49–96) was not removed from its position simply because Syb-(1–52) was not able to bind to the ΔN complex, we labeled Syb-(1–52) at its extra C-terminal cysteine residue with the fluorescent dye Alexa-488. Upon mixing of the labeled Syb-(1–52) with the ΔN complex, a rapid change in fluorescence was monitored, demonstrating that Syb-(1–52) is able to bind efficiently. At pseudo-first-order conditions, the rate of assembly was ≈123,000 M^{-1}s^{-1} (supplemental Fig. 2*a*). These findings are consistent with our previous observation that two non-overlapping synaptobrevin fragments can bind at the same time, forming a complex that structurally resembles the extended four-helix SNARE bundle (30). Note, however, that in the earlier study we used different fragments, Syb1–59 and Syb60–96 (see supple-

FIGURE 1. **Calorimetric titrations of the three neuronal SNARE proteins.** All isothermal calorimetric experiments were performed at 25 °C in phosphate buffer, pH 7.4. In each figure, the *top panel* shows the base-line-corrected raw data in power *versus* time during the injections. The *lower panel* displays the integrated areas normalized to the amount of the injectant (kcal mol^{-1}) *versus* its molar ratio to the protein(s) in the cell. The *solid lines* represent the best fit to the data using a nonlinear least squares fit using either a one-set-of-sites or a two-sets-of-sites model. The results of the fits are given in Table 1. For each experiment, a representative thermogram is shown, but note that all experiments were performed in replicate. *a*, illustration of the reaction pathways of ternary SNARE complex formation. The helical regions of the SNARE proteins are depicted schematically as boxes (*blue*, *red*, and *green* for synaptobrevin 2, syntaxin 1a, and SNAP-25a, respectively; note that SNAP-25 has two helices that are connected by a long, flexible linker that is not depicted). In addition, the known on- and off-rates are given (30, 31) Note that the schema is used to illustrate the complexes formed during the reaction steps investigated by ITC in *b–e*. *b*, titration of SNAP-25 (25.5 μM) into SyxH3 (3.2 μM). In this orientation of the binding experiment, apparently only one transition can be observed, yet the profile can also be fitted to a two-sets-of-sites binding model that is able to distinguish between the two binding steps. Note that the *top panel* also contains ITC runs in which Syb (23 μM) was titrated into SNAP-25 (3 μM) and into SyxH3 (3 μM), resulting only in background heat of dilution (*i.e.* no detectable binding occurs). *c*, titration of SyxH3 (57.4 μM) into SNAP-25 (5 μM). The profile of the reversed titration displays two distinct binding steps. Note that dissociation of the SyxH3 oligomers produces additional small, negative heat changes. The titration of SyxH3 into the buffer was used to correct for this effect. *d*, titration of SNAP-25 (15 μM) into a mix of SyxH3 (2 μM) and Syb-(1–96) (10 μM). Note that an excess of Syb-(1–96) was used to ensure that all SyxH3-SNAP-25 complexes were readily converted to ternary complexes. However, similar results were obtained using an equimolar mix of SyxH3 and Syb-(1–96). *e*, titration of a stoichiometric mix of Syb-(1–96) (15 μM) and SyxH3 into SNAP-25 (1.7 μM). Note that the titrations following the procedure used in *b* and *d* were also carried out at different temperatures. To obtain the heat capacity change for binding, the apparent binding enthalpy (ΔH) is plotted as a function of temperature (supplemental Fig. 1).

Energetics of SNARE Complex Formation

TABLE 1

Thermodynamic parameters of the interaction of the neuronal SNARE proteins measured by ITC at 25 °C

The experimental ITC data are shown in Fig. 1 and in supplemental Fig. 3. No binding was detected for the titrations of SyxH3 and Syb and of SNAP-25 and Syb. For the injection of SNAP-25 into SyxH3 and into SyxH3 and Syb1–96, only the values of a one-set-of-sites fit are given. ΔN complex, Syb-(49–96)·SyxH3·SNAP-25 complex; Syb-(1–70) complex, Syb1–70·SyxH3·SNAP-25.

Cell	Syringe	Fit model	K_D	ΔH	$-T\Delta S$	ΔG	N
			nM	kcal mol^{-1}	kcal mol^{-1} K^{-1}	kcal mol^{-1}	
SyxH3	SNAP-25	1-site	64.9 ± 17.1	−41.3 ± 1.0	31.5	−9.8	1.88
SNAP-25	SyxH3	2-site	4.3 ± 4.2	−46.9 ± 7.2	35.5	−11.4	0.21
			233.6 ± 64.3	−31.0 ± 1.8	22.0	−9.0	1.21
SyxH3/Syb-(1–96)	SNAP-25	1-site	22.8 ± 6.1	−112.8 ± 2.5	102.4	−10.4	0.97
SNAP-25	SyxH3/Syb-1–96	2-site	4.3 ± 5.5	−60.5 ± 16.8	49.1	−11.4	0.28
			29.9 ± 6.5	−148.9 ± 12.0	138.6	−10.2	0.41
ΔN complex	Syb-1–96	1-site	2.1 ± 0.6	−29.9 ± 0.3	18.1	−11.8	1.05
ΔN complex	Syb-1–87	1-site	5.4 ± 1.8	−26.3 ± 0.4	15.0	−11.3	0.96
ΔN complex	Syb-1–65	1-site	5.7 ± 1.2	−18.1 ± 0.2	6.9	−11.2	0.97
ΔN complex	Syb-1–52	1-site	18.3 ± 2.0	−22.7 ± 0.2	12.1	−10.6	1.03
Syb-(1–70) complex	Syb7-1–96	1-site	1368.0 ± 293.0	−6.0 ± 0.3	−2.0	−8.0	0.89
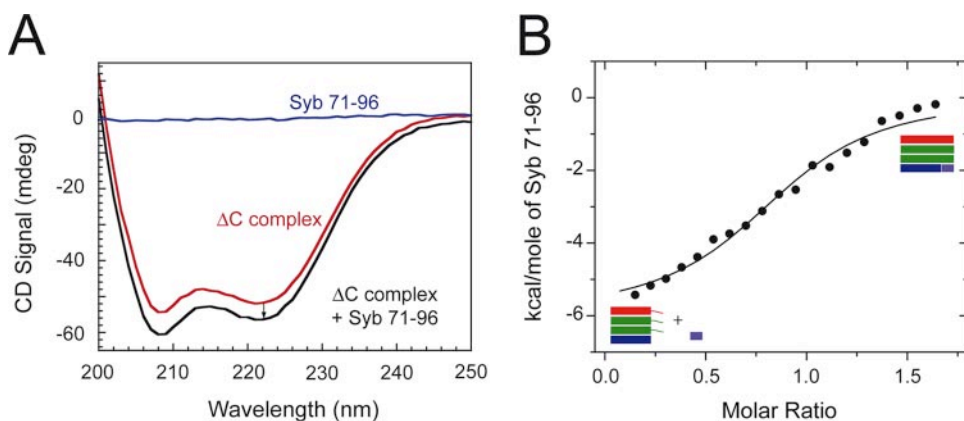
FIGURE 3. **Binding of the very C-terminal region of the synaptobrevin coil is reversible.** *a*, changes in the CD spectrum upon mixing of purified Syb-(1–70) complex (5 μM) with Syb-(71–96) peptide (10 μM). The spectrum of the mix was recorded after 1 h incubation at room temperature. *b*, calorimetric titration of Syb-(71–96) (105 μM) into the purified Syb-(1–70) complex (Syb-(1–70)·SyxH3·SNAP-25; 15 μM).

mental Fig. 2*c* and a supplemental section for a detailed comparison of the stabilities of the Syb-(1–52)·Syb-(49–96) complex and the Syb1–59·Syb60–96 complex).

Reversible Binding of the N-terminal Coil of Synaptobrevin to the ΔN Complex—The binding of different synaptobrevin fragments to the ΔN complex produced favorable enthalpic changes that saturated at a 1:1 molar ratio (Table 1; for comparison, the ITC results for the titration of SNAP-25 into a mix of the synaptobrevin fragments with SyxH3 are given in supplemental Table 1; see also supplemental Fig. 3). Interestingly, the apparent affinity and enthalpic change was somewhat reduced for the Syb-(1–87) fragment as compared with Syb-(1–96). The binding of the shorter Syb-(1–65) fragment to the ΔN complex was even somewhat less affine and resulted in less pronounced enthalpic changes compared with the Syb-(1–87) fragment. Similar results were obtained for the binding of the non-replacing Syb-(1–52) fragment (Fig. 2*b*), which took place at 23 nM affinity (Table 1). We have shown above that the Syb-(1–52) fragment does not displace the bound C-terminal fragment, Syb-(49–96) (Fig. 2*c*). Consequently, the ITC data reflect only binding to the preformed N-terminal binding site of the ΔN complex. Surprisingly, we observed no clear difference in the ITC profiles of Syb-(1–65) compared with Syb-(1–52) (Table 1; supplemental Fig. 3, *h* and *i*). It might be tempting to speculate that the thermodynamic profiles of the synaptobrevin fragments reflect an incremental zippering process. However,

because the shorter fragment Syb-(1–65) displaces the bound Syb-(49–96) fragment from the ΔN complex more slowly than the longer Syb-(1–96) and Syb-(1–87) (Fig. 2*c*), it is likely that the ITC approach did not record the slow heat change of the displacement step for these fragments.

Up to this point we have assumed that ITC did not provide the true energetics of the synaptobrevin binding step because the assembly process is essentially irreversible. Now, however, the question arose of whether the binding of Syb-(1–52) to the ΔN complex may be reversible, as the C-terminal Syb-(49–96) fragment can remain bound, thereby keeping the entire complex together. To record this step, we used labeled Syb-(1–52), which dissociated at a rate of about 0.0006 s^{-1} from the ΔN complex (supplemental Fig. 2*b*). The ratio of off- and on-rates result in an affinity of about 5 nM, confirming the affinity determined by the ITC measurements.

Energetics of the C-terminal Zippering Step—Finally, to investigate the energetics of the C-terminal zippering step, we used a ternary SNARE complex containing a C-terminal-truncated synaptobrevin fragment, Syb-(1–70), and monitored binding of the Syb-(71–96) peptide to the free C-terminal portion of complex. Previous investigations had suggested that the C-terminal portion of the Syb-(1–70) complex is less structured (30). We employed CD spectroscopy to test whether the association of the Syb-(71–96) peptide to the Syb1–76 complex would induce additional structure. Indeed, we observed a small increase in α-helical content upon mixing of the Syb-(1–70) complex and Syb-(71–96) peptide (Fig. 3*a*). We then used ITC to assess the energetics of the reaction. Compared with the ITC measurements described so far, we observed a relatively small enthalpy of binding ($\approx$−6 kcal/mol) upon titrating the Syb-(71–96) peptide into the purified Syb-(1–70) complex. The affinity of the association was about 1.4 μM. This suggests that zippering of the very C-terminal end of the bundle contributes only moderately to the force of the process. However, it should

be kept in mind that the energy contribution of this portion might be considerably higher with an intact synaptobrevin coil.

DISCUSSION

In the synapse the core of the membrane fusion machinery consists of the three SNARE proteins, syntaxin 1a, SNAP-25, and synaptobrevin 2. Although these proteins have been intensively studied, the central question of how their sequential assembly into a trans-complex drives the fusion of the vesicle with the plasma membrane still remains unanswered (for review, see Refs. 1–7). Here, we have investigated the energetics of complex formation involving the soluble portion of the neuronal SNARE proteins using ITC. The major goal of this work was to build a solid thermodynamic foundation for improved understanding of how the energy released during complex formation can be harnessed for membrane fusion. Using kinetic investigations as a basis, the following assembly pathway has previously been put forward; in an initial, rate-limiting step, the two plasma membrane SNAREs, syntaxin and SNAP-25, assemble into a transient 1:1 heterodimer, which in turn provides a high affinity binding site for the vesicular synaptobrevin (30, 31). Indeed, this assembly pathway is strongly corroborated by our thermodynamic investigations, suggesting that it corresponds to the series of intermediate stages through which the assembling SNAREs pass *in vivo*.

Large Enthalpic Changes Drive SNARE Complex Formation—Earlier spectroscopic investigations have shown that SNARE complex formation is attended by large structural rearrangements. As the interacting domains of the individual proteins are mostly disordered and the resulting complexes, either the 2:1 complex or the ternary SNARE complex, have an extended four-helix bundle structure (8–10, 32–34), the assembly reaction can be described as coupled folding and binding. Our ITC investigations revealed that assembly is driven by large favorable enthalpic changes (ΔH), reflecting the extensive intermolecular interface established during the reaction. The enthalpic change is counterbalanced by the large entropic costs ($-T\Delta S$) associated with the disorder-to-order transition. Although it has long been thought that proteins have a three-dimensional fold dictated by their amino acid sequence, it has been established more recently that numerous proteins contain long disordered segments under physiological conditions (for review, see Refs. 35 and 36). Many intrinsically disordered proteins fold into stable structures only upon binding to their targets. Their inherent flexibility enables these proteins to form extensive binding surfaces, often by binding to multiple partners in a multiprotein complex. Coupled folding and binding has been found in molecules with various functions. The SNARE complex assembly reaction, which uses assembly energy to bring two membranes into close apposition, adds a new facet to the versatility of unfolded proteins.

Notably, to the best of our knowledge the enthalpic changes of ≈110 kcal/mol recorded for the formation of the ternary SNARE complex are among the largest observed for protein-protein interactions so far. Remarkably, large enthalpic changes also occur within the interaction of the human immunodeficiency virus envelope glycoprotein with the cellular CD4 receptor (37, 38), a reaction that initiates the fusion of the viral

membrane with the cellular plasma membrane. Envelope glycoprotein is composed of the surface (gp120) and the transmembrane (gp41) subunits. The binding of the gp120 glycoprotein to CD4 is coupled to an extensive structural rearrangement that leads to the activation of the co-receptor binding site (39, 40). Upon binding to the coreceptor (41), this conformational change of gp120 is transmitted to gp41, which then reorganizes itself into a fusogenic configuration. The actual driving force for viral membrane fusion is thought to be the formation of a highly stable six-helical bundle structure by gp41 (42, 43). The assembly passes through a "prehairpin" intermediate that is thought to consist of a central trimeric coiled coil formed by N-terminal heptad repeats; note that gp41 is present as a trimer. Antiparallel packing of the three C-terminal heptad repeats to the trimeric core pulls the viral and cellular membranes together (for review, see Refs. 44–47). Hence, both membrane fusion machineries, the SNAREs and envelope glycoprotein, undergo large conformational changes that culminate in the formation of a tight helix bundle structure that pulls two membranes together.

On the surface it seems that both machineries employ the same "energetic strategy" to fuse membranes, but it should be noted that there are also fundamental differences in both mechanisms. First, the topology of SNARE proteins relative to the opposing membranes is different from that of viral fusion proteins, which reside only in the viral membrane. Then, viral fusion proteins like envelope glycoprotein store their energy in a so-called metastable configuration, which arises from the proteolytic cleavage of the precursor, gp160. Consequently, the viral fusion proteins can undergo the conformational change only once. Conversely, the SNAREs remain in an unfolded configuration that can snap into a tight complex upon contact. The energy set free during the SNARE assembly process is "recycled" by the disassembly reaction catalyzed by the ATPase *N*-ethylmaleimide. Hence, in contrast to the viral fusion machinery, the cellular SNARE machinery can be re-used. Still, it is striking that in both fusion reactions, highly stable helix bundles are used, although they seem to be the product of convergent evolution. This suggests that this structure constitutes a relatively simple assembly mechanism to generate force.

A Transient Syntaxin-SNAP-25 Heterodimer Serves as Intermediate—During SNARE complex formation, the two plasma membrane proteins syntaxin and SNAP-25 are believed to provide the binding site for the vesicular synaptobrevin. Indeed, of all the possible binary combinations, only these two proteins were found to form a tight complex (8, 9). Hence, synaptobrevin binding requires a structural rearrangement of syntaxin and SNAP-25. However, *in vitro* they tend to reside in a complex with 2:1 stoichiometry in which the binding site for synaptobrevin is occupied by a second syntaxin molecule (8, 31). Our ITC investigations show that the 2:1 complex is the predominant entity at higher nanomolar concentrations, whereas the 1:1 heterodimer forms at lower nanomolar concentrations. The large enthalpic changes suggest that the formation of the 1:1 heterodimer is accompanied by major conformational changes. It should be noted that because of the limitations of the standard ITC analysis method, the contributions of both reaction steps to the enthalpy of binding were not

Energetics of SNARE Complex Formation

resolved precisely. Thus, it remains unclear how much surface is buried during this step.

Although the general outline of the assembly pathway of the neuronal SNARE proteins is widely accepted, some few aspects are controversial, one of them being the configuration of the syntaxin-SNAP-25 assembly in the membrane. Although structural investigations have demonstrated that they form a 2:1 complex in solution, it has been claimed that the two proteins form a 1:1 entity when co-expressed and inserted into artificial membranes (48). It should be noted, however, that if co-expressed, syntaxin and SNAP-25 in fact resided in a 1:1 configuration, much faster liposome fusion rates should be observable when this complex is used (14). One, therefore, has to assume that the coexpressed complex does not reside in a conformation that supports immediate synaptobrevin binding. It should also be noted that earlier EPR studies have shown that the membrane inserted syntaxin-SNAP-25 complex has a 2:1 configuration as well (49), although in this study only the H3 region of syntaxin was used. In the 2:1 configuration, the slow fusion rates can be explained easily by competition between the second syntaxin and synaptobrevin for binding. That the 2:1 complex does not actually offer a reactive synaptobrevin binding site was demonstrated recently when its liposome fusion activity was compared with the ΔN complex, which allowed for much quicker fusion (30).

Micro-reversibility of Synaptobrevin Binding—According to our earlier investigations, the SNARE assembly process essentially becomes irreversible upon association of the synaptobrevin (25). So far, it has been unclear at which point synaptobrevin binding becomes quasi-irreversible. Previous investigations showed that the C-terminal portion of synaptobrevin can bind reversibly as long as the complex is held together by the N-terminal portion (30). Remarkably, using the ΔN complex we have demonstrated that binding of the N-terminal coil of synaptobrevin is reversible as well. One should bear in mind, however, that reversibility was found only when fragments were used rather than when the entire coil of synaptobrevin was used. Obviously, the intact synaptobrevin helix is much more stably bound than the fragments, and consequently, its dissociation would be too slow to be measured. In addition, our approach is not able for detecting when only a portion of the synaptobrevin coil detached. Single molecule techniques and molecular dynamics (see *e.g.* Ref. 50) would provide better means to observe such events.

Note that reversible binding of the N-terminal portion of synaptobrevin was found only when the C-terminal region of the complex was held together by a fragment of synaptobrevin. For topological reasons, this setting probably does not occur *in vivo*. Hence, it might be argued that our reductionist approach, which assesses the thermodynamic and kinetic properties of the molecules involved, does not reflect the cellular situation. However, a situation can be envisioned in which the binding site of synaptobrevin in the 1:1 heterodimer is maintained by the action of other molecules. For example, we have recently shown that the protein Munc18 tightly controls the formation of the syntaxin-SNAP-25 complex (51). Along with other factors, the task of Munc18 might be to organize and control the formation of the synaptobrevin binding site. In fact, the inter-

action of syntaxin and SNAP-25 is very slow, suggesting that *in vivo* "priming" factors are required to orchestrate the reaction so it can overcome its large activation barrier. At first glance, this appears to be a major investment, but it should also be considered that a relatively labile synaptobrevin acceptor site ensures that the fusion reaction can be tightly controlled *in vivo*.

Assessing the Free Energy of SNARE Complex Formation— The free energy of SNARE complex formation cannot be assessed conventionally (25). However, the energy stored in the SNARE bundle (or more precisely in about three-quarter of the bundle) has recently been estimated to be around 35 k_BT (equivalent to about 20 kcal/mol) by either atomic force microscopy or SFA measurements (29). This extraordinarily high energy would imply that the affinity of the SNARE complex is in the low femtomolar range and is one of the most stable protein complexes observed so far. When we investigated the SNARE assembly by ITC, however, we only observed affinities in the range of about 1 nM (equivalent to about 11 kcal/mol; note that a 10-fold change in binding constant corresponds to ≈1.4 kcal/mol) no matter which reaction pathway we examined. How can this large difference be explained?

It is well known that atomic force microscopy experiments are carried out under non-equilibrium conditions and, thus, do not measure the *bona fide* free energy of SNARE complex formation. Nonetheless, it is puzzling why, for example, vastly different rates of spontaneous dissociation of ternary SNARE complexes of ≈158 years (26) and ≈2.1 s (27, 28) were reported or why very similar high stabilities were measured for the interaction of syntaxin and synaptobrevin, although these two SNARE proteins do not form a tight complex (Fig. 1*b*) (9). These inconsistencies raise the possibility that handling of SNARE proteins might be still very critical for single-molecule approaches (for a comprehensive assessment of the different approaches see Ref. 52). Henceforth, we will, thus, compare only the SFA and ITC equilibrium approaches.

Previous investigations have shown that the folding equilibrium of SNARE complexes cannot be reached within an experimentally affordable time, suggesting that the ITC measurements underestimated the binding constant. We noticed, however, that the SFA measurements might have been affected by the same problem. These experiments measured approach/separation cycles involving two lipid surfaces, one of which had the synaptobrevin anchored within it, whereas the other provided the anchor for the coexpressed syntaxin SNAP-25 complex (29, 53). Strikingly, these revealed diverging profiles of the approach and separation phases that bear strong resemblance to the non-coinciding folding and unfolding transitions observed by standard denaturation protocols (25). Although the proteins appear to assemble progressively during the approaching phase, once the complex is assembled, it seems to resist separation until it suddenly breaks apart. Notably, a plateau was reached after about 60 min. This time period does not correspond to equilibrium but, rather, suggests that after this time, the SFA instrument, like the ITC instrument, is not sensitive enough beyond this point to detect further subliminal changes. Nonetheless, it remains unclear why the energetics obtained by ITC and by SFA measurements are vastly different.

We noted, however, that with the SFA approach the number of pulling complexes had to be deduced rather indirectly to calculate the free energy assigned to a single SNARE complex. Hence, although the SFA measurements describe the SNARE assembly and disassembly cycle between membranes very well, it seems possible that the energetic contribution of the SNARE assembly is overestimated.

How Do SNAREs Catalyze Membrane Fusion?—According to the zipper model, progressive assembly of SNARE complexes may culminate in a release of energy that is sufficient to drive membrane merging. The earliest step at which SNARE complex formation would be able to provide energy for pulling the membranes together is upon engagement of synaptobrevin with the 1:1 heterodimer. It should be kept in mind, however, that the affinity of the 1:1 heterodimer formation gives an upper limit for the subsequent engagement of synaptobrevin. Our data suggest that the N-terminal coil of synaptobrevin can bind reversibly to the N-terminal region of the syntaxin-SNAP-25 heterodimer. It is conceivable that this configuration corresponds to a stable assembly that the SNAREs form between two opposing membranes. N-terminal association is then followed by assembly of the C-terminal portion of the four-helix bundle. Interestingly, our measurements suggest that the energy released during the very C-terminal zipper process is smaller than during N-terminal assembly. Thus, our data corroborate the notion that C-terminal zippering might be reversible, suggesting that assembly of the trans-SNARE complex might be balanced by the repulsive forces of the two membranes.

In addition, the question of how many SNARE complexes are needed to fuse two membranes has been discussed intensively over the years. As outlined before, according to the stalk hypothesis, a large activation energy of about $40\,k_BT$ needs to be provided by the SNARE assembly process. The extraordinary stability measured by the SFA implies that only a few, maybe even only one, complex would need to join forces to fuse membranes (29), whereas the lower stability measured here by ITC appears to imply that a larger number of SNARE complexes have to cooperate. In this regard, it is interesting to note that a single human immunodeficiency virus fusion protein releases a similar amount of energy to the SNARE complex during zippering as the affinity of the outer-layer peptide for a trimeric inner core of gp41 was determined to be around 3.6 nM (54). Moreover, it should be kept in mind that the high free energy of the transition state of membrane fusion inferred by the stalk model is controversial, as the model does not account for the activity of proteins, which probably modulate the fusion pathway (23, 24). Also, the stalk model treats lipid membranes as an elastic surface, although biological membranes are crowded with proteins (55). For example, in synaptic vesicles (the organelle in which synaptobrevin 2 is located) about a quarter of the entire membrane volume is taken up by transmembrane domains, suggesting that the majority of lipid molecules are not free (56).

The putative energy landscape of SNARE complex formation between membranes is schematically drawn in Fig. 4. Clearly, this scenario is speculative, as our results shed light only on the assembly energy of the soluble portions of the neuronal SNAREs. Thus, to understand whether SNARE assembly
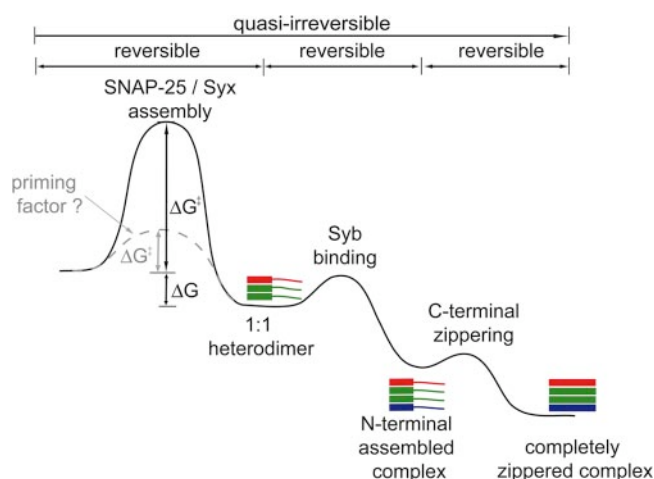
FIGURE 4. **Energy profile of SNARE complex assembly reaction.** Simplified energy diagram of the sequential assembly steps of the neuronal SNARE proteins. The individual reactions are reversible, yet the entire assembly process is essentially irreversible. In a rate-limiting reaction the two plasma membrane SNAREs, syntaxin and SNAP-25, assemble into a transient 1:1 syntaxin-SNAP-25 heterodimer. Lowering of the large activation energy of this step is probably orchestrated by additional factors *in vivo*. The syntaxin-SNAP-25 heterodimer offers a binding site for the vesicular synaptobrevin, a step that joins the two membranes intended to fuse. Eventually, the C-terminal region of the four-helix bundle assembles, bringing the two membranes into close proximity.

indeed provides the mechanical force to fuse membranes, it is necessary to understand how the assembly force is transmitted through the transmembrane domains into the membrane. Unfortunately, little is known about the structure of the linker region between the core SNARE complex and the transmembrane domains. It should also be kept in mind that although the SNARE proteins were anchored in lipid bilayers in the SFA experiments, anchoring was achieved by an artificial lipid anchor attached C-terminally. Hence, the approach is not suited to determine the force transmitted across lipid bilayers. Clearly, although we do not exactly understand how the SNARE assembly force is harnessed for membrane fusion, models of this process will remain speculative.

REFERENCES
1. Jahn, R., and Scheller, R. H. (2006) *Nat. Rev. Mol. Cell Biol.* **7,** 631–643
2. Wojcik, S. M., and Brose, N. (2007) *Neuron* **55,** 11–24
3. Verhage, M., and Toonen, R. F. (2007) *Curr. Opin. Cell Biol.* **19,** 402–408
4. Yoon, T. Y., and Shin, Y. K. (2008) *Cell. Mol. Life Sci.* **3,** 460–469
5. Malsam, J., Kreye, S., and Sollner, T. H. (2008) *Cell. Mol. Life Sci.* **65,** 2814–2832
6. Rizo, J., and Rosenmund, C. (2008) *Nat. Struct. Mol. Biol.* **15,** 665–674
7. Martens, S., and McMahon, H. T. (2008) *Nat. Rev. Mol. Cell Biol.* **9,** 543–556
8. Fasshauer, D., Bruns, D., Shen, B., Jahn, R., and Brünger, A. T. (1997) *J. Biol. Chem.* **7,** 4582–4590
9. Fasshauer, D., Otto, H., Eliason, W. K., Jahn, R., and Brünger, A. T. (1997) *J. Biol. Chem.* **272,** 28036–28041
10. Sutton, R. B., Fasshauer, D., Jahn, R., and Brunger, A. T. (1998) *Nature* **395,** 347–353

Energetics of SNARE Complex Formation

11. Hanson, P. I., Heuser, J. E., and Jahn, R. (1997) *Curr. Opin. Neurobiol.* **7,** 310–315
12. Weber, T., Zemelman, B. V., McNew, J. A., Westermann, B., Gmachl, M., Parlati, F., Sollner, T. H., and Rothman, J. E. (1998) *Cell* **92,** 759–772
13. Parlati, F., Weber, T., McNew, J. A., Westermann, B., Sollner, T. H., and Rothman, J. E. (1999) *Proc. Natl. Acad. Sci. U. S. A.* **96,** 12565–12570
14. Melia, T. J., Weber, T., McNew, J. A., Fisher, L. E., Johnston, R. J., Parlati, F., Mahal, L. K., Sollner, T. H., and Rothman, J. E. (2002) *J. Cell Biol.* **158,** 929–940
15. Lu, X., Zhang, F., McNew, J. A., and Shin, Y. K. (2005) *J. Biol. Chem.* **280,** 30538–30541
16. Xu, Y., Zhang, F., Su, Z., McNew, J. A., and Shin, Y. K. (2005) *Nat. Struct. Mol. Biol.* **12,** 417–422
17. Chen, X., Arac, D., Wang, T. M., Gilpin, C. J., Zimmerberg, J., and Rizo, J. (2006) *Biophys. J.* **90,** 2062–2074
18. Dennison, S. M., Bowen, M. E., Brunger, A. T., and Lentz, B. R. (2006) *Biophys. J.* **90,** 1661–1675
19. Yoon, T. Y., Okumus, B., Zhang, F., Shin, Y. K., and Ha, T. (2006) *Proc. Natl. Acad. Sci. U. S. A.* **103,** 19731–19736
20. Yoon, T. Y., Lu, X., Diao, J., Lee, S. M., Ha, T., and Shin, Y. K. (2008) *Nat. Struct. Mol. Biol.* **15,** 707–713
21. Giraudo, C. G., Garcia-Diaz, A., Eng, W. S., Yamamoto, A., Melia, T. J., and Rothman, J. E. (2008) *J. Biol. Chem.* **283,** 21211–21219
22. Martens, S., Kozlov, M. M., and McMahon, H. T. (2007) *Science* **316,** 1205–1208
23. Jahn, R., and Grubmüller, H. (2002) *Curr. Opinion Cell Biol.* **14,** 488–495
24. Chernomordik, L. V., and Kozlov, M. M. (2008) *Nat. Struct. Mol. Biol.* **15,** 675–683
25. Fasshauer, D., Antonin, W., Subramaniam, V., and Jahn, R. (2002) *Nat. Struct. Biol.* **9,** 144–151
26. Yersin, A., Hirling, H., Steiner, P., Magnin, S., Regazzi, R., Huni, B., Huguenot, P., De los Rios, P., Dietler, G., Catsicas, S., and Kasas, S. (2003) *Proc. Natl. Acad. Sci. U. S. A.* **100,** 8736–8741
27. Liu, W., Montana, V., Bai, J., Chapman, E. R., Mohideen, U., and Parpura, V. (2006) *Biophys. J.* **91,** 744–758
28. Liu, W., Montana, V., Parpura, V., and Mohideen, U. (2008) *Biophys. J.* **95,** 419–425
29. Li, F., Pincet, F., Perez, E., Eng, W. S., Melia, T. J., Rothman, J. E., and Tareste, D. (2007) *Nat. Struct. Mol. Biol.* **14,** 890–896
30. Pobbati, A., Stein, A., and Fasshauer, D. (2006) *Science* **313,** 673–676
31. Fasshauer, D., and Margittai, M. (2004) *J. Biol. Chem.* **279,** 7613–7621
32. Margittai, M., Fasshauer, D., Pabst, S., Jahn, R., and Langen, R. (2001) *J. Biol. Chem.* **276,** 13169–13177
33. Xiao, W., Poirier, M. A., Bennett, M. K., and Shin, Y. K. (2001) *Nat. Struct. Biol.* **8,** 308–311
34. Zhang, F., Chen, Y., Kweon, D. H., Kim, C. S., and Shin, Y. K. (2002) *J. Biol. Chem.* **277,** 24294–24298
35. Dyson, H. J., and Wright, P. E. (2005) *Nat. Rev. Mol. Cell Biol.* **6,** 197–208
36. Fink, A. L. (2005) *Curr. Opin. Struct. Biol.* **15,** 35–41
37. Myszka, D. G., Sweet, R. W., Hensley, P., Brigham-Burke, M., Kwong, P. D., Hendrickson, W. A., Wyatt, R., Sodroski, J., and Doyle, M. L. (2000) *Proc. Natl. Acad. Sci. U. S. A.* **97,** 9026–9031
38. Leavitt, S. A., SchOn, A., Klein, J. C., Manjappara, U., Chaiken, I. M., and Freire, E. (2004) *Curr. Protein Pept. Sci.* **5,** 1–8
39. Kwong, P. D., Wyatt, R., Robinson, J., Sweet, R. W., Sodroski, J., and Hendrickson, W. A. (1998) *Nature* **393,** 648–659
40. Liu, J., Bartesaghi, A., Borgnia, M. J., Sapiro, G., and Subramaniam, S. (2008) *Nature* **455,** 109–113
41. Huang, C. C., Lam, S. N., Acharya, P., Tang, M., Xiang, S. H., Hussan, S. S., Stanfield, R. L., Robinson, J., Sodroski, J., Wilson, I. A., Wyatt, R., Bewley, C. A., and Kwong, P. D. (2007) *Science* **317,** 1930–1934
42. Lu, M., Blacklow, S. C., and Kim, P. S. (1995) *Nat. Struct. Biol.* **2,** 1075–1082
43. Weissenhorn, W., Dessen, A., Harrison, S. C., Skehel, J. J., and Wiley, D. C. (1997) *Nature* **387,** 426–430
44. Eckert, D. M., and Kim, P. S. (2001) *Annu. Rev. Biochem.* **70,** 777–810
45. Weiss, C. D. (2003) *AIDS Rev.* **5,** 214–221
46. Weissenhorn, W., Hinz, A., and Gaudin, Y. (2007) *FEBS Lett.* **581,** 2150–2155
47. Harrison, S. C. (2008) *Nat. Struct. Mol. Biol.* **15,** 690–698
48. Rizo, J. (2008) *Structure* **16,** 163–165
49. Kim, C. S., Kweon, D. H., and Shin, Y. K. (2002) *Biochemistry* **41,** 10928–10933
50. Durrieu, M. P., Lavery, R., and Baaden, M. (2008) *Biophys. J.* **94,** 3436–3446
51. Burkhardt, P., Hattendorf, D. A., Weis, W. I., and Fasshauer, D. (2008) *EMBO J.* **27,** 923–933
52. Parpura, V., and Mohideen, U. (2008) *Trends Neurosci.* **31,** 435–443
53. Rizo, J., and Dai, H. (2007) *Nat. Struct. Mol. Biol.* **14,** 880–882
54. Frey, G., Rits-Volloch, S., Zhang, X. Q., Schooley, R. T., Chen, B., and Harrison, S. C. (2006) *Proc. Natl. Acad. Sci. U. S. A.* **103,** 13938–13943
55. Engelman, D. M. (2005) *Nature* **438,** 578–580
56. Takamori, S., Holt, M., Stenius, K., Lemke, E. A., Gronborg, M., Riedel, D., Urlaub, H., Schenck, S., Brugger, B., Ringler, P., Muller, S. A., Rammner, B., Grater, F., Hub, J. S., De Groot, B. L., Mieskes, G., Moriyama, Y., Klingauf, J., Grubmuller, H., Heuser, J., Wieland, F., and Jahn, R. (2006) *Cell* **127,** 831–846
57. Fasshauer, D., Antonin, W., Margittai, M., Pabst, S., and Jahn, R. (1999) *J. Biol. Chem.* **274,** 15440–15446

Supplementary information

Is assembly of the SNARE complex enough to fuel membrane fusion?

Katrin Wiederhold and Dirk Fasshauer

Comparing the stabilities of the Syb1–52:Syb49–96 and Syb1–59:Syb60–96 complexes

Our finding that a stable Syb1–52:Syb49–96 complex can be formed is consistent with our previous observation that two non-overlapping synaptobrevin fragments can bind at the same time to form a complex that structurally resembles the extended four-helix bundle SNARE complex. In the earlier study, we used a complex containing the fragments Syb1-59 and Syb60-96, which were produced by proteolytic cleavage by the light chain of botulinum neurotoxin D (BoNT/D) (Pobbati et al. 2006). In both complexes, the break in the synaptobrevin helix renders the complex less stable. On first glance, the reversible association of the Syb1-52 fragment to N-terminal side of the ΔN complex - thus forming the Syb1–52:Syb49–96 complex - appears to be somewhat in conflict with our earlier investigations on the Syb1–59:Syb60–96 complex. In the latter complex, we had observed that the C-terminal half, rather than the N-terminal half, of synaptobrevin can dissociate and rebind as long as the complex is hold together. These findings had evoked a scenario for neurosecretion in which SNARE complex formation can be arrested halfway (Pobbati et al. 2006). How then, can it be explained that in one complex the N-terminal peptide (i.e. the Syb1–52:Syb49–96 complex) can bind reversibly but in the other complex (i.e. the Syb1–59:Syb60–96 complex), it is the C-terminal peptide that can bind reversibly? A relatively simple explanation is suggested by the different lengths of the synaptobrevin fragments used in the two complexes. In the Syb1–52:Syb49–96 complex, the C-terminal synaptobrevin fragment is significantly longer (≈ 3 helix

turns) than in the Syb1–59:Syb60–96 complex, suggesting that the C-terminal portion of the Syb1–52:Syb49–96 complex might be stabilized, possibly being more stable than its N-terminal portion.

To test this idea, we investigated the stability of the two regions of the Syb1–52:Syb49–96 complex using CD spectroscopy. For these investigations, we used different complexes (the ΔN complex containing Syb49-96, with and without Syb1-52, and a ternary complex containing Syb1-52 only) and compared the melting curves with our earlier investigations on the Syb1–59:Syb60–96 complex. Detailed interpretations of the resulting melting curves are given in the legend to Suppl. Fig.2c. Nevertheless, together our data corroborate the idea that the C-terminal portion of the Syb1–52:Syb49–96 complex unfolds at higher temperatures than its N-terminal portion, explaining why the N-terminal fragment can dissociate more easily than the C-terminal fragment in this complex. Because the C-terminal synaptobrevin fragment can dissociate reversibly in the Syb1-59:Syb60-96 complex, we first sought to use this setting to investigate the energetics of the C-terminal zippering process. However, it was difficult to purify the two fragments and assemble monodisperse Syb1–59:Syb60–96 complexes reliably.

Reference:

Pobbati, A., A. Stein, et al. (2006). "N- to C-terminal SNARE complex assembly promotes rapid membrane fusion." <u>Science</u> **313**(5787): 673-676.

Supplementary figures
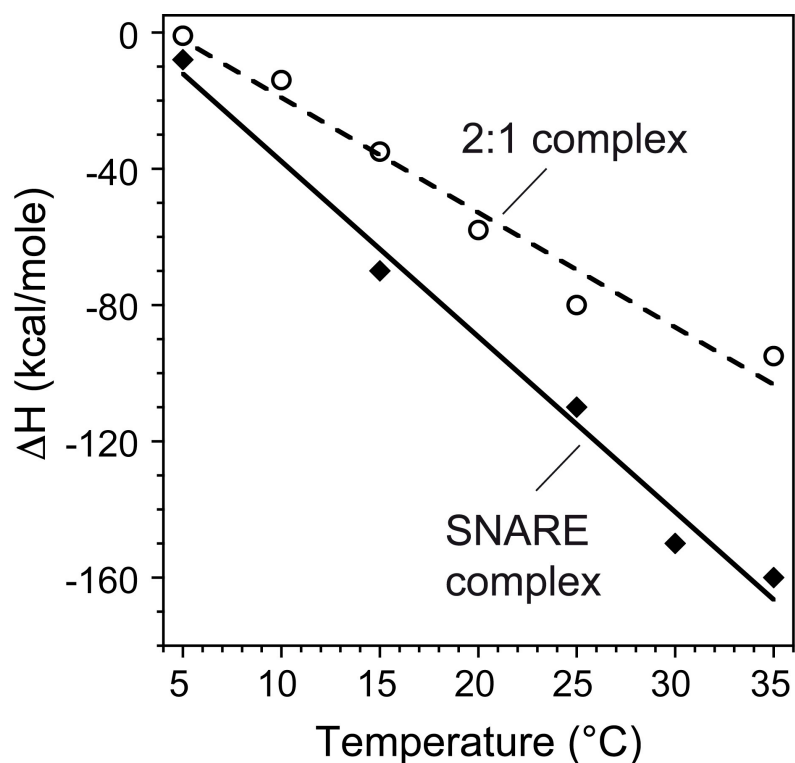
Suppl. Fig. 1: Heat capacity change of binding.

ITC experiments in which SNAP-25 was titrated into SyxH3 (open circles) or into a mix of SyxH3 and Syb1-96 (filled squares) were performed at different temperatures. The enthalpy of binding (ΔH) was obtained by fitting the data to a one-site binding model and plotted as a function of temperature for each of the binding reactions. Solid lines represent linear least-square fits where the slopes are the heat capacity change of binding (ΔCp). The large negative heat capacity changes of about -3372 kcal mol^{-1} for the assembly of the SyxH3:SNAP-25 complex and -5145 kcal mol^{-1} for the assembly of the ternary SNARE complex (SyxH3:SNAP-25:Syb1-96) probably reflect major structural rearrangements coupled with binding.
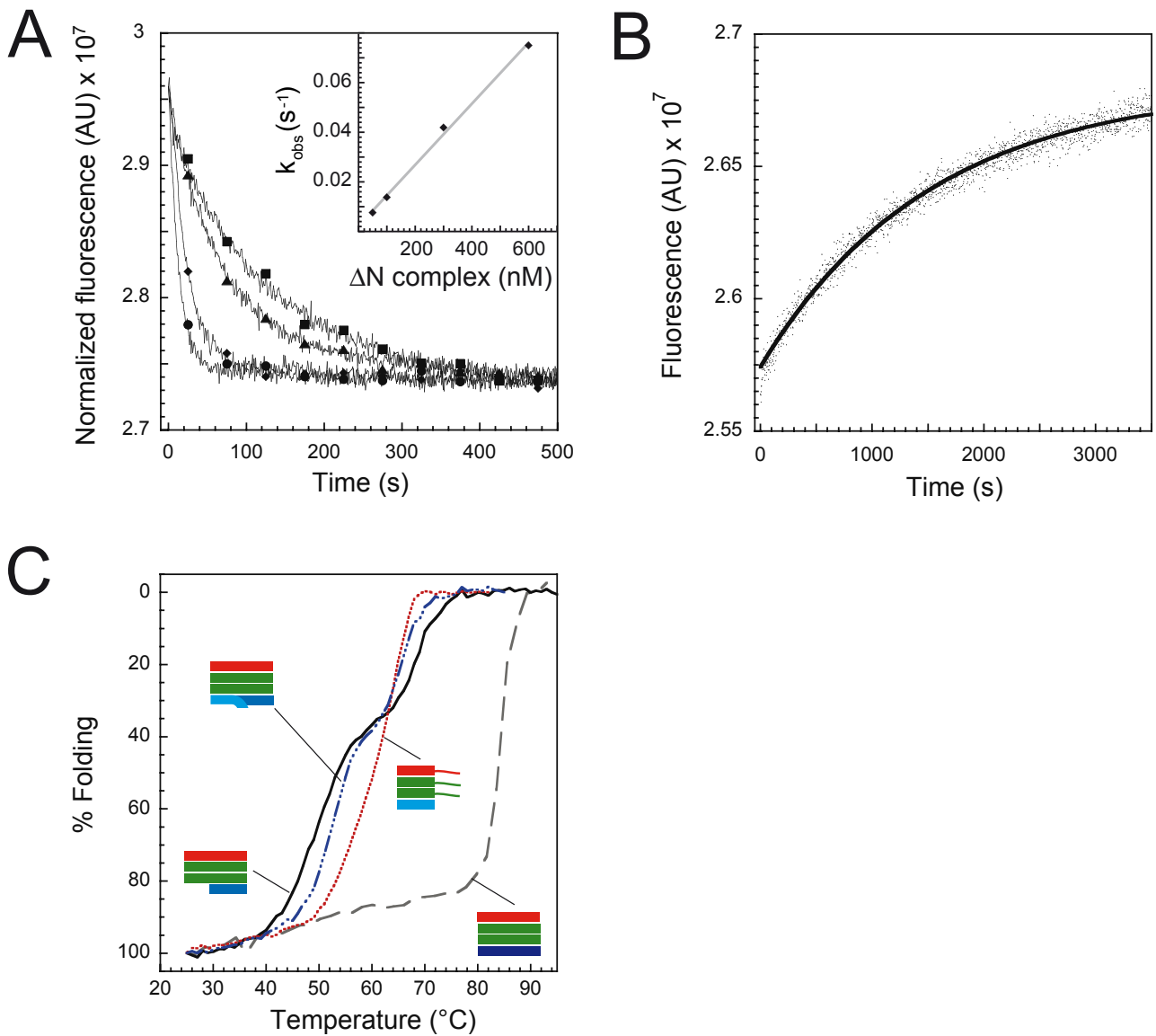
A) Binding of Syb1-52 to the ΔN complex (Syb49–96:SyxH3:SNAP-25). Syb1-52 was labeled with the fluorescent dye Alexa 488 at an additional C-terminal cysteine residue (Syb1-52^{C53Alexa488}).

B) Dissociation of Syb1-52 from the ΔN complex (Syb49–96:SyxH3:SNAP-25) by competitive dissociation. We first mixed 50 nM labeled Syb1-52 (Syb1-52^{C53Alexa488}) with the same amount of unlabelled ΔN complex. After binding was completed, we added a large excess of unlabelled Syb1-52 to record dissociation of the labeled fragment by competitive displacement.

C) Thermal unfolding of SNARE complexes containing the synaptobrevin fragments Syb1-52 and Syb49-96. Thermal denaturation of the purified ternary complexes containing Syb1-52 (Syb1-52:SyxH3:SNAP-25), Syb49-96 (Syb49–96:SyxH3:SNAP-25; i.e. the ΔN complex),

and a premix of the ΔN complex and Syb1-52 (mixed approximately at a 1: 1.5 ratio), resulting in a Syb1–52:Syb49–96 complex, was monitored by CD spectroscopy at 222 nm. The ternary complex containing Syb1-52 unfolded at about 62 °C, whereas thermal denaturation of the ΔN complex occurred in two steps at $T_{m1} \approx 50$ °C and $T_{m2} \approx 65$ °C. It is very likely that the first melting point of the ΔN complex denotes the unfolding of its N-terminal portion, which, according to our model, consists only of the N-terminal regions of syntaxin and SNAP-25. The second melting transition probably denotes the unfolding of the remaining portion of the complex, held together by Syb49-96. When we monitored the denaturation of the premixed Syb1–52:Syb49–96 complex, we again observed a two-step unfolding process. In contrast to the isolated ΔN complex, however, the first unfolding transition occurred at a slightly elevated temperature, whereas the second unfolding transition occurred at slightly lower temperature. It seems that binding of Syb1-52 to the ΔN complex renders the N-terminal portion of the complex slightly more stable and weakens the C-terminal portion somewhat. This suggests that the C-terminal portion of the Syb1–52:Syb49–96 complex unfolds at higher temperatures than its N-terminal portion, explaining why the N-terminal fragment can dissociate more easily than the C-terminal fragment. Employing CD spectroscopy, we found earlier that the thermal denaturation of the Syb1–59:Syb60–96 complex occurs in two steps as well. However, we were able to demonstrate that in the first unfolding transition, at ≈ 45 °C, the C-terminal portion of the complex unfolded. By contrast, the N-terminal portion of the complex was more stable ($T_m \approx 65$ °C). Interestingly, a ΔN complex containing Syb60-96 unfolds only in one step at $T_m \approx 45$ °C. Taken together this suggests that the C-terminal portion of the Syb1–52:Syb49–96 complex is more stable than that of the Syb1–59:Syb60–96 complex.
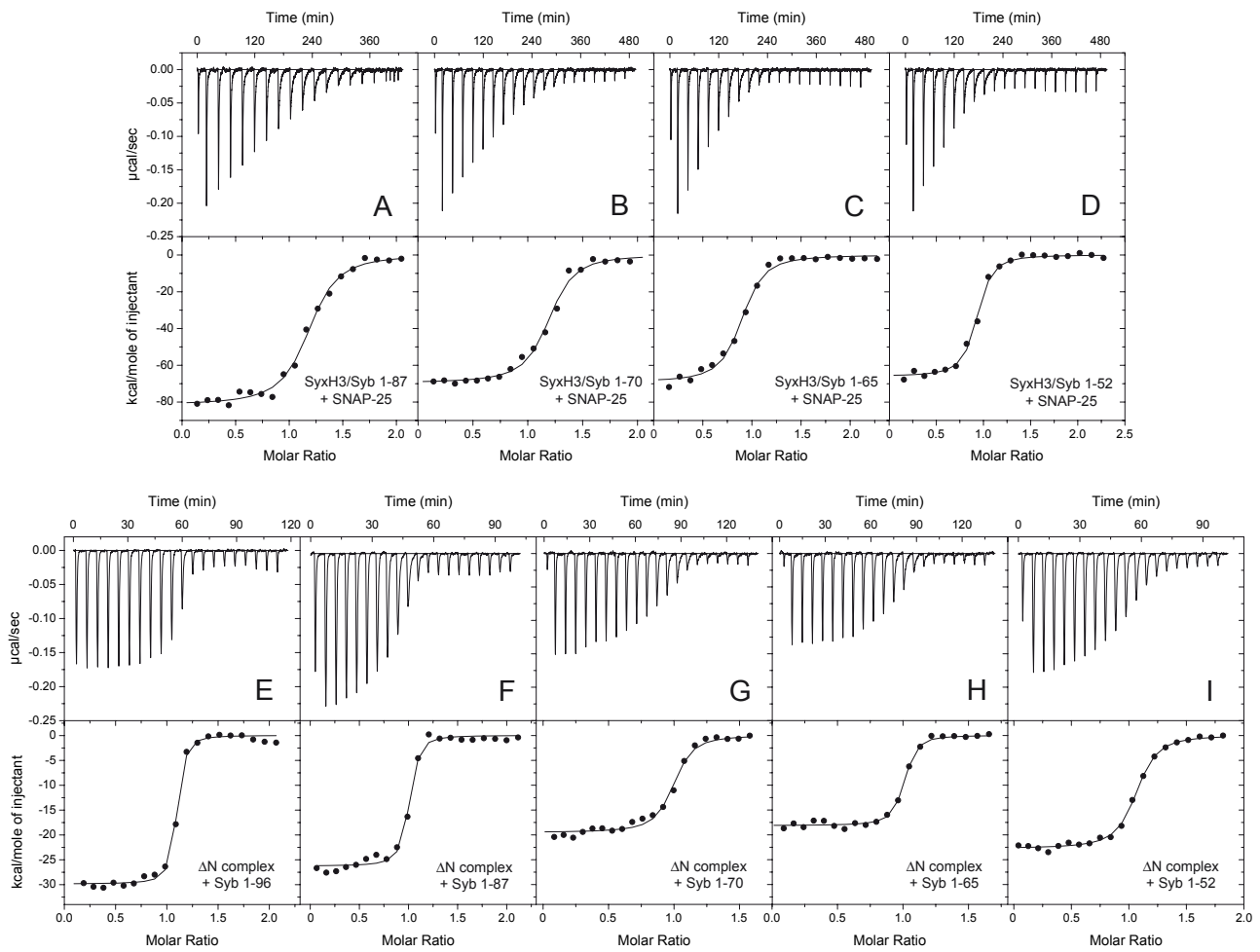
Suppl. Fig. 3 - Isothermal titration calorimetry data for the ternary SNARE complex formation using synaptobrevin fragments.

All ITC experiments were performed at 25 °C in phosphate buffer, pH 7.4. In each panel, the top panel shows the base-line corrected raw data in power versus time during the injections. The lower panel displays the integrated areas normalized to the amount of the injectant (kcal mol^{-1}) versus its molar ratio to the protein(s) in the cell. The solid lines represent the best fit to the data using a nonlinear least squares fit. The results of the fits are given in Table 1 and Suppl. Table 1. For each experiment, a representative thermogram is shown, but note that all experiments were performed in replicate.

A-D) Titration of SNAP-25 into a mix of SyxH3 and different synaptobrevin fragments.

E-I) Titration of different synaptobrevin fragments into the purified ΔN complex.

cell	syringe	K_D (nM)	DH (kcal mol^{-1})	-TDS (kcal mol^{-1} K^{-1})	DG (kcal mol^{-1})	N
SyxH3/ Syb1-87	SNAP-25	30.0 ± 5.0	-81.4 ± 1.2	71.1	-10.3	1.15
SyxH3/ Syb1-70	SNAP-25	21.6 ± 4.4	-69.5 ± 1.1	59.0	-10.5	1.16
SyxH3/ Syb1-65	SNAP-25	28.3 ± 5.8	-69.0 ± 1.3	58.7	-10.3	0.86
SyxH3/ Syb1-52	SNAP-25	13.1 ± 2.5	-65.9 ± 0.9	55.2	-10.7	0.89
ΔN complex	Syb1-70	15.2 ± 3.6	-19.5 ± 0.3	8.8	-10.7	0.97

Suppl. Table 1: Thermodynamic parameters of binding of different synaptobrevin fragments measured by ITC at 25 °C.